Heliyon 10 (2024) e36293

Contents lists available at ScienceDirect

Heliyon

journal homepage: www.cell.com/heliyon

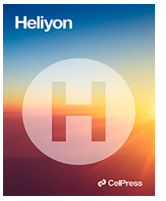

Research article

Pyrolysis kinetics of waste ryegrass under nitrogen and air atmosphere

Yonglin Wu [a], Ming Jiang [a], Yichun Liu [a], Yishu Deng [b,*]

[a] College of Resources and Environment, Yunnan Agricultural University, Kunming, 650201, China
[b] College of Architecture and Engineering, Yunnan Agricultural University, Kunming, 650201, China

ARTICLE INFO

Keywords:
Ryegrass
Biomass
Pyrolysis
Air atmosphere
Nitrogen atmosphere
Kinetic

ABSTRACT

To investigate the pyrolysis reaction of ryegrass, we conducted a simultaneous thermal analysis using thermogravimetric(TG) analyzers. This involved obtaining data through Thermogravimetry (TG), Derivative Thermogravimetry (DTG), and Differential thermal analysis (DTA) techniques. The experiments were conducted under dynamic nitrogen and air atmospheres at different heating rates. The kinetic parameters of ryegrass pyrolysis were determined using the Kissinger method, the Flynn-Wall-Ozawa (FWO) peak conversion rate approximate equivalence method, the Flynn-Wall-Ozawa (FWO) equal conversion rate method, and the Škvára-Šesták (S–S) method. It provides a theoretical basis for the reuse of ryegrass resources. The findings indicated that the pyrolysis temperature of ryegrass increased with the accelerated rate of temperature increase in both atmospheres. The average weight loss rate of pyrolysis of ryegrass in the air atmosphere (92.27 %) is higher than that compared to that in a nitrogen atmosphere (86.11 %). Additionally, the temperature required for complete decomposition is lower in the former case. The FWO peak conversion rate approximation equivalence approach and the FWO equal conversion rate method do not apply to the solution of the pyrolysis activation energy of ryegrass. The pyrolysis activation energy for the two decomposition stages, as calculated by the Kissinger method, is 165.73 and 185.86 kJ/mol^{-1} in the air atmosphere, and 219.99 and 277.02 kJ/mol^{-1} in a nitrogen atmosphere, respectively. The activation energy and mechanism function of ryegrass pyrolysis calculated by using the S–S method are as follows: $[-\ln(1-\alpha)]^2$, 119.79, 104.31, 95.75, and 91.93 kJ/mol^{-1} in air atmosphere, $(1-\alpha)^{-1}$, 176.64, 67.89, 61.15, and 54.25 kJ/mol^{-1} in nitrogen atmosphere, respectively. The activation energy of ryegrass pyrolysis, as determined by both the Kissinger method and S–S method, was found to be higher under an air atmosphere compared to a nitrogen atmosphere.

1. Introduction

The perennial ryegrass (Ryegrass L.) is a herbaceous species in the ryegrass family that exhibits extensive adaptability, including its high fertility, well-developed root system, high tillering capacity, ease of cultivation, and ability to grow in harsh conditions such as cold, acidic, alkaline, and hypersaline soils, among others [1,2]. Ryegrass is a suitable grass for animal feed in temperate grassland agriculture due to its high nutritious value and easy digestibility by animals [3]. Additionally, ryegrass can be utilized for

* Corresponding author.
E-mail address: 13987627051@163.com (Y. Deng).

https://doi.org/10.1016/j.heliyon.2024.e36293
Received 16 December 2023; Received in revised form 9 August 2024; Accepted 13 August 2024
Available online 14 August 2024

phytoremediation to enrich soil with heavy metals and metalloids such as zinc, arsenic, cadmium, and lead[4–6]. When ryegrass is used for phytoremediation, it absorbs heavy metals from the soil, which renders it unfit for animal husbandry and composting thereafter. Due to the presence of heavy metals, discarded ryegrasses have a high likelihood of contaminating soil and water bodies if not properly managed. Therefore, it is necessary to reuse these discarded ryegrasses to prevent environmental pollution that would occur if disposed of as regular solid waste. The purpose of this paper is to evaluate the possibility of pyrolysis of waste ryegrass under aerobic and anaerobic conditions, and to provide theoretical reference for biomass reuse of waste ryegrass.

The pyrolysis of biomass involves the decomposition of polymer chains inside biomass macromolecules, resulting in the creation of bio-oil, non-condensable gas, and biochar [7,8]. The raw materials commonly used for biomass pyrolysis are agricultural waste derived from lignocellulosic biomass [9]. Currently, the primary focus of biomass pyrolysis research is on understanding the pyrolysis characteristics of different types of biomass and determining the related kinetic parameters through the analysis of the resulting products on the overall pyrolysis process [10,11]. The pyrolysis activation energy and kinetic parameters commonly used can be calculated using many methods, such as the Kissinger method [12], Flynn-Wall-Ozawa(FWO) method [13], dynamic mechanical analysis (DMA) method [14], Coats-Redfern(CR) method [15] and Friedman method [16]. In addition, new pyrolysis technologies, including microwave pyrolysis [17], solar pyrolysis [18], co-pyrolysis [19], and catalytic pyrolysis [20] have been developed to optimize biomass pyrolysis. Ryegrass composition consists of crude fibers, fibers, and hemifibers, which are promising materials for biomass energy. Through pyrolysis, the fiber components in ryegrass can be converted into biomass energy. This process also allows for the examination of the pyrolysis characteristics and mechanism of ryegrass, potentially enabling the reuse of its resources [21]. A detailed study of waste ryegrass pyrolysis is lacking, however, certain researchers have used thermogravimetric analyzers to investigate the pyrolysis characteristics and mechanisms of comparable biomass waste materials, such as tea stalks [22] and wood chips [23,24]. The research aims to offer fundamental data and technological guidance for the effective utilization of biomass wastes. The study employed thermogravimetric analysis (TG-DTA) to compare and analyze the pyrolysis process of ryegrass under a dynamic air atmosphere and nitrogen atmosphere. Additionally, the study calculated the kinetic parameters of the pyrolysis process. The purpose of this analysis was to provide data reference for the thermochemical conversion of waste ryegrass for resource utilization.

2. Materials and methods

2.1. Experimental materials

Waste ryegrass was collected from the greenhouse located behind Yunnan Agricultural University.

2.2. Experimental method

A certain amount of freshly harvested ryegrass leaves was measured by weight and designated as M1. The recently harvested ryegrass leaves were subjected to a drying process in an oven at 105 °C for 30 min. Subsequently, the leaves were further dried at a temperature of 75 °C for 48 h. Once completely dried, the weight of the dried sample was measured, and its mass was recorded as M2. The moisture content of ryegrass, as determined by formula (1), is 74.9 %. The calculation formula for the moisture content of ryegrass (1) is as follows:

$$Moisture\ content = \frac{(M1 - M2)}{M1} \times 100\% \tag{1}$$

The HCT-1 synchronous TG-DTA thermal analyzer from Beijing Hengjiu Experimental Equipment Co., Ltd. was used to determine the TG-DTG and TG-DTA curves of ryegrass samples. The experimental conditions included a sample mass of 3.5 ± 0.1 mg, dynamic nitrogen atmosphere, and air atmosphere, both with an airflow rate of 50 mL/min. The heating rate varied at 5 °C/min, 10 °C/min, 15 °C/min, 20 °C/min, while the temperature range was set from 50 °C–700 °C, respectively.

2.3. Kinetic methods of pyrolysis

2.3.1. Basic theory of pyrolysis kinetics

The pyrolysis of ryegrass is a type of solid pyrolysis reaction, which can be represented by equation (2) [25]:

$$\frac{d\alpha}{dt} = A \exp\left(-\frac{E}{RT}\right) f(\alpha) \tag{2}$$

Where: The α-conversion rate at any moment t during the pyrolysis of ryegrass is calculated using the formula %, $\alpha=(m_0-m_t)/(m_0-m_f)$ [26],m_0、 m_t、 m_f represent the mass of the sample at the beginning, at any moment t, and the termination of the sample, respectively. The g; t-pyrolysis time, s; A-response index prefactor,s^{-1}; E-pyrolysis activation energy, kJ/mol; R-universal gas constant, equal to 8.314J/mol·K; T-pyrolysis temperature, K; $f(\alpha)$- represents the Differential Dynamics Mechanism Functions.

2.3.2. Calculation of pyrolysis activation energy

The activation energy, E, for the pyrolysis process of ryegrass under different atmospheres, was determined using various methods including the Kissinger method [27], Flynn-Wall-Ozawa(FWO) peak conversion rate approximate equivalence method [28],

Table 1
Selection of Mechanism functions.

No.	G(α)	No.	G(α)
1	α^2	9	$-\ln(1-\alpha)$
2	$\alpha+(1-\alpha)\ln(1-\alpha)$	10~16	$[-\ln(1-\alpha)]^n$ (n = 2/3, 1/2, 1/3, 4, 1/4, 2, 3)
3	$(1-2/3\alpha)-(1-\alpha)^{2/3}$	17~22	$1-(1-\alpha)^n$ (n = 1/2, 3, 2, 4, 1/3, 1/4)
4~5	$[1-(1-\alpha)^{1/3}]^n$ (n = 2, 1/2)	23~27	α^n (n = 1, 3/2, 1/2, 1/3, 1/4)
6	$[1-(1-\alpha)^{1/2}]^{1/2}$	28	$(1-\alpha)^{-1}$
7	$[(1-\alpha)^{1/3}-1]^2$	29	$(1-\alpha)^{-1}-1$
8	$[(1/(1-\alpha)^{1/3})-1]^2$	30	$(1-\alpha)^{-1/2}$

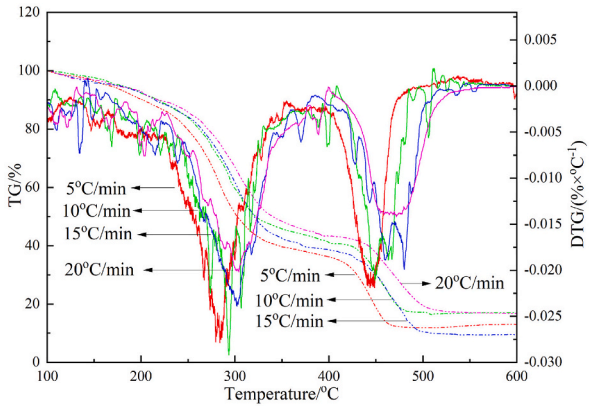

Fig. 1. TG-DTG curves of ryegrass at different heating rates in N_2 atmospheres.

Flynn-Wall-Ozawa(FWO) same conversion rate method [29], Škvára-Šesták(S–S) method [30]. These methods were employed to analyze the TG/DTG curves and investigate the reaction rate of the pyrolysis process. The equations known as the Kissinger, FWO, and S–S are shown in (3), (4), and (5).

$$\ln\left(\frac{\beta}{T_{\max}^2}\right)=\ln\left(\frac{A_K R}{E_K}\right)-\frac{E_K}{RT_{\max}} \tag{3}$$

$$\lg\beta=\lg\left[\frac{A_O E_O}{RG(\alpha)}\right]-2.315-0.4567\frac{E_O}{RT_\alpha} \tag{4}$$

$$\lg G(\alpha)=\lg\frac{A_S E_S}{R\beta}-2.315-0.4567\frac{E_S}{RT} \tag{5}$$

Where: T_{max}-Peak decomposition temperature, K; β-heating rate, K/min or °C/min; $G(\alpha)$为30 mechanism functions [31] (Table 1); T_α-Temperature at which the same conversion is achieved at different heating rates, K; E_K, E_O, E_S and A_K, A_O, A_S represent the activation energy of pyrolysis and the reaction finger front factor for the Kissinger, FWO, and S–S equations respectively The remaining parameters in equation (1) have the same physical significance.

Kissinger method: According to equation (2), $1/T_{\max}$ was used as the horizontal coordinate and, $\ln(\beta/T^2max)$ as the vertical coordinate to make a linear fitting straight line. The activation energy E_K for pyrolysis was determined by calculating the slope of $-E_K/R$, and the $\ln(A_K)$ was obtained from the intercept $\ln(A_K R/E_K)$.

FWO: Approximate Equivalence of Peak Conversion Rates. This method implies that the conversion rate $\alpha_{\max}$ at the peak pyrolysis temperature $T_{\max}$ is approximately equal at different heating rates β and can be substituted for T_α in equation (3) with $T_{\max}$. A linear fitting line is obtained using $1/T_{\max}$ as the horizontal coordinate and $\lg\beta$ as the vertical coordinate. The activation energy of pyrolysis, E_O, can be determined by calculating the slope of $-0.4567E_O/R$. When the peak conversion rates $\alpha_{\max}$ are not equal, this method is not applicable. The peak conversion rate $\alpha_{\max}$ is determined using the formula $\alpha_{\max}=(m_0-m_{t(max)})/(m_0-m_f)$, where $m_{t(max)}$ represents the mass of the sample corresponding to the peak decomposition temperature $T_{\max}$.

FWO iso conversion rate method: At different heating rates β, a series of the same conversion rates α (range from 10 % to 90 % with a step of 10 %) are selected. Given the values of α, m_0, m_f are known, m_t can be determined using inverse deduction according to the formula $\alpha=(m_0-m_t)/(m_0-m_f)$. The T_α value can be obtained using the data of m_t and TG curves. Finally, a linear fitting is performed using $1/T_\alpha$ as the transverse coordinate and $\lg\beta$ as the longitudinal coordinate. The slope of the resulting straight line with the same reason of the fitting $-0.4567E_O/R$, represents the activation energy E_O.

Corresponding to each heating rate β and the mechanism function $G(\alpha)$, linear regression is performed using $1/T$ as the horizontal

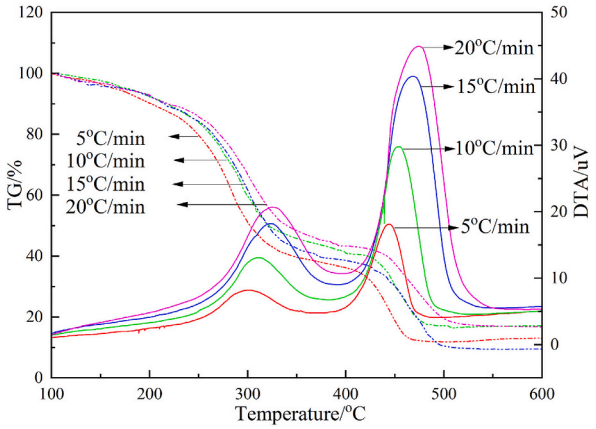

Fig. 2. TG-DTA curves of ryegrass at different heating rates in N_2 atmospheres.

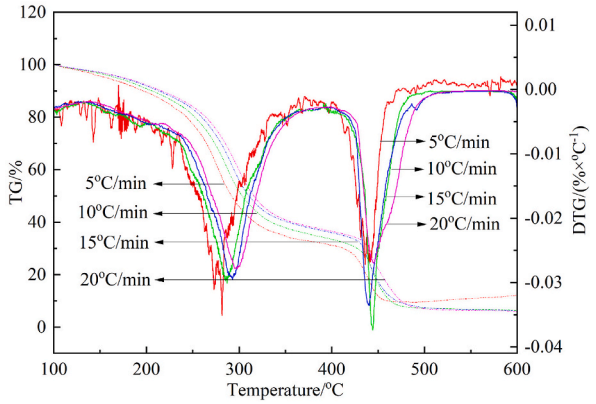

Fig. 3. TG-DTG curves of ryegrass at different heating rates in air atmospheres.

coordinate and $\lg G(\alpha)$ as the vertical coordinate, and E_s, $\lg A_s$ are calculated from the slope of the straight line $-0.4567\ E_S/R$ and the intercept $\lg(A_S E_S/R\beta)$-2.315, and screened to satisfy the following conditions [32] $G(\alpha)$ with E_s in the range of 0–400 kJ-mol^{-1}, $(E_S-E_O)E_O \leq 0.22$. Additionally, the $\lg A_S$ corresponding to the E_s values that meet these parameters should have a range of $|(\lg A_S-\lg A_K)/\lg A_K| \leq 0.30$.

3. Results and analysis

3.1. Characterization of pyrolysis of ryegrass under nitrogen atmosphere

The TG-DTG and TG-DTA curves of the pyrolysis of ryegrass in a nitrogen atmosphere are shown in Figs. 1 and 2, respectively. The figures demonstrate that the weight loss, rate of ryegrass pyrolysis was 87.88 %, 83.35 %, 90.34 %, and 82.85 % at the heating rates of 5 °C/min, 10 °C/min, 15 °C/min, and 20 °C/min, respectively. The average weight loss rate was 86.11 %. It is evident that the heating rate affects the percentage of weight loss of ryegrass pyrolysis. Too high or too low heating rate is not conducive to the pyrolysis of ryegrass. When the heating rate is 15 °C/min, the percentage of weight loss reaches the peak. The average percentage of weight loss was 86.11 %. The percentage of weight loss of ryegrass did not exhibit any significant changes under different heating rates, indicating that the heating rate had no obvious impact on the percentage of weight loss of ryegrass. However, with the increase of heating rate, the DTG curve moves to the high temperature area. Additionally, the DTA curve displayed two upward exothermic peaks, indicating that both stages of weight loss involved exothermic reactions. The DTA curve exhibited two upward exothermic peaks, indicating that both weight loss stages of ryegrass were exothermic and both peaks were positively correlated with the rate of heating. The initial peak occurred within the temperate range of 200 and 350 °C, signifying the decomposition of a significant quantity of hemicellulose and a smaller amount of cellulose in ryegrass. The second peak, observed between 400 and 550 °C, indicated a large amount of cellulose and crude fiber decomposition. This behavior closely resembled the pyrolysis process of Pennisetum purpureum Schumach studied by Li et al. [33]. With an increase in the heating rate, the TG, DTG, and DTA curves shifted towards higher temperatures. During the decomposition of ryegrass, as the percentage of weight loss becomes equal, a higher heating rate corresponds to a higher

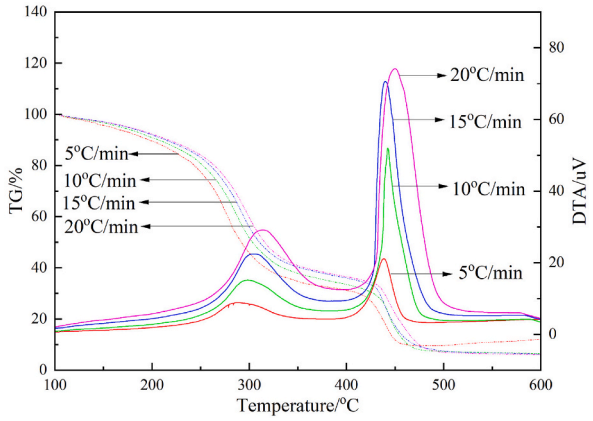

Fig. 4. TG-DTA curves of ryegrass at different heating rates in air atmospheres.

Table 2
The basic data of the kinetics by TG/DTG curves in N_2 atmospheres.

Decomposition stage	β /K·min^{-1}	T_{max} /°C	T_{max} /K	$\ln(\beta/T_{max}^2)$	$(1/T_{max}) \times 10^3$ /K^{-1}	m_o /mg	m_f /mg	$m_{t(max)}$ /mg	α_{max} /%
First stage	5	284.13	557.28	−11.037	1.79	3.5	0.63	2.35	40.06
	10	293.48	566.63	−10.38	1.76	3.5	0.99	2.65	33.98
	15	302.02	575.18	−10.00	1.74	3.5	0.92	2.69	31.03
	20	304.10	577.26	−9.72	1.73	3.5	0.95	2.62	34.51
Second stage	5	443.75	716.9	−11.54	1.39	3.5	0.63	1.01	86.93
	10	448.91	722.06	−10.86	1.38	3.5	0.99	1.51	79.63
	15	459.84	732.99	−10.49	1.36	3.5	0.92	1.49	77.75
	20	472.22	745.37	−10.23	1.34	3.5	0.95	1.37	83.57

Table 3
The basic data of the kinetics by TG/DTG curves in air atmospheres.

Decomposition stage	β /K·min^{-1}	T_{max} /°C	T_{max} /K	$\ln(\beta/T_{max}^2)$	$(1/T_{max}) \times 10^3$ /K^{-1}	m_o /mg	m_f /mg	$m_{t(max)}$ /mg	α_{max} /%
First stage	5	281.8	554.95	−11.03	1.80	3.5	0.33	1.90	50.47
	10	287.52	560.67	−10.36	1.78	3.5	0.46	2.18	43.42
	15	292.62	565.77	−9.97	1.77	3.5	0.54	2.24	42.57
	20	297.68	570.83	−9.70	1.75	3.5	0.44	2.16	43.79
Second stage	5	426.15	699.30	−11.49	1.43	3.5	0.33	0.94	80.76
	10	436.07	709.219	−10.83	1.41	3.5	0.46	1.18	76.32
	15	441.18	714.33	−10.43	1.40	3.5	0.54	1.32	73.65
	20	446.56	719.71	−10.16	1.39	3.5	0.44	1.25	73.53

decomposition temperature and a broader interval of weight loss.

3.2. Pyrolysis characteristics of ryegrass in air atmosphere

Fig. 3 displays the TG-DTG curve of ryegrass pyrolysis in the presence of air, while Fig. 4 shows the TG-DTA curve. The figure shows that the percentage of weight loss of ryegrass are 87.4 %, 93.72 %, 93.97 %, and 93.98 %, when the heating rates are 5 °C/min, 10 °C/min, 15 °C/min, and 20 °C/min, respectively. In an air atmosphere, the average percentage of weight loss is 92.27 %. The initial weight loss peak of the DTG curve decreases as the heating rate increases, but the second weight loss peak is not affected by it. Both peaks of the curve exhibit an increase with the increase in heating rate. When comparing the two scenarios, it was discovered that under the same heating rate, the ryegrass experienced a higher rate of weight loss in an air atmosphere compared to a nitrogen atmosphere. Additionally, the temperature needed for complete decomposition was lower in the air atmosphere. Furthermore, the two peaks on the DTA curve were larger, indicating a more intense exothermic reaction.

Typically, the duration required for biomass to achieve the final pyrolysis temperature decreases as the heating rate increases. Increasing the heating rate is beneficial for biomass pyrolysis [34]. In the air atmosphere, the pyrolysis weight loss rate of ryegrass is the highest under the condition of the fastest heating rate in the air atmosphere, and the pyrolysis weight loss rate of ryegrass is the highest in the fastest heating rate, which aligns with previous research findings. However, certain studies have found that increasing

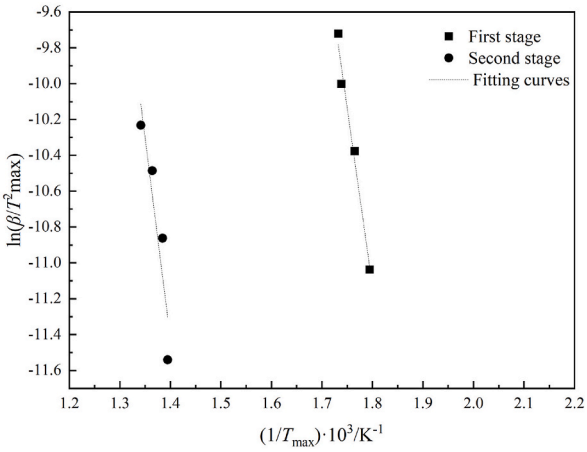

Fig. 5. Fitting curves of $\ln(\beta/T_{max}^2)$-$1/T_{max}$ in N_2 atmospheres.

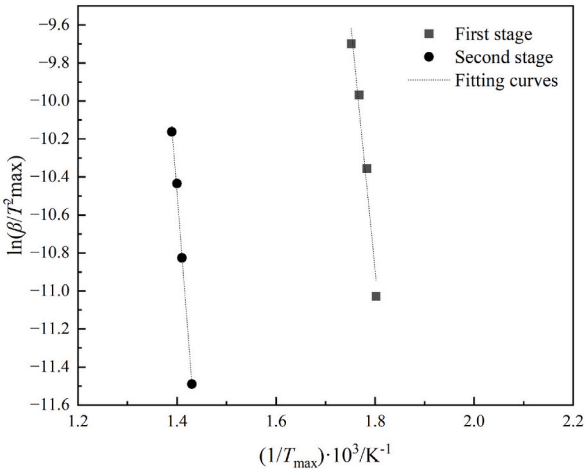

Fig. 6. Fitting curves of $\ln(\beta/T_{max}^2)$-$1/T_{max}$ in air atmospheres.

the heating rate leads to an increase in the temperature difference between the internal and external surfaces of biomass, thereby causing a thermal lag effect. Consequently, when the heating rate increases, the biomass experiences a decrease in weight loss and the residual weight is larger [35]. Under a nitrogen atmosphere, the ryegrass exhibits the highest rate of weight loss during pyrolysis when heated at a rate of 15 °C/min. The possible explanation is that a heating rate of 5 °C/min, and 15 °C/min promotes the pyrolysis of ryegrass. However, when compared to a heating of 20 °C/min, the thermal lag effect of 15 °C/min is smaller.

3.3. Pyrolysis kinetics of ryegrass

The basic kinetic data acquired from the TG-DTG curve analysis of ryegrass in nitrogen and air atmosphere are shown in Tables 2 and 3, respectively. The linear equation derived using the Kissinger method is shown in Figs. 5 and 6. Based on the fitting results shown in Fig. 5, the fitting equation for the nitrogen atmosphere is as follows: In the first weightlessness stage, the equation for Y = −19.93X+24.75. The correlation coefficient is R = 0.9757. The pyrolysis activation energy is E = 165.73 kJ/mol, and the exponential factor logarithm lnA = 27.74; In the second weightlessness stage, the equation for Y = −22.35X+19.87. The correlation coefficient is R = 0.7899. The pyrolysis activation energy is E = 185.86 kJ/mol, and the exponential factor logarithm is lnA = 22.97. The fitting result of Fig. 6 indicates that in air atmosphere, the fitting equation for the first weightlessness stage is Y = −26.46X+36.74. The correlation coefficient is R = 0.9719, the calculated pyrolysis activation energy is E = 219.99 kJ/mol, and the exponential factor logarithm is lnA = 40.02. In the second weightlessness stage, the fitting equation is Y = −33.32X+36.16. The correlation coefficient is R = 0.9968, the pyrolysis activation energy is E = 277.02 kJ/mol, and the exponential factor logarithm is lnA = 36.91.

Refer to Tables 2 and 3 for the peak conversion values of α_{max} calculated using the approximate equivalence method of FWO peak conversion. By examining Tables 2 and 3 and it is evident that α_{max} decreased as the heating rate increased during the same decomposition stage, regardless of whether it was in a nitrogen atmosphere or an air atmosphere. This suggests that the pyrolysis

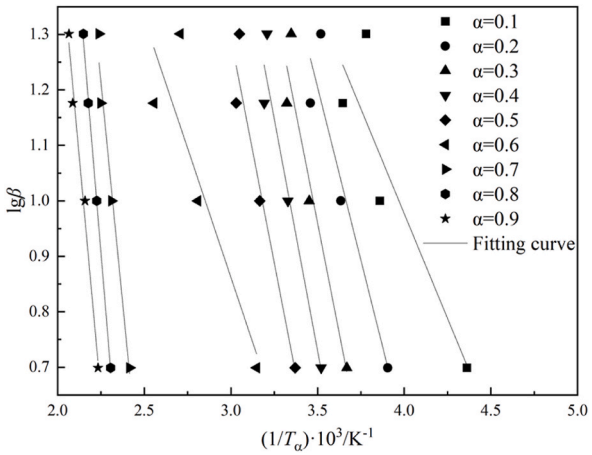

Fig. 7. Fitting curves of lgβ-1/T_α in N_2 atmospheres.

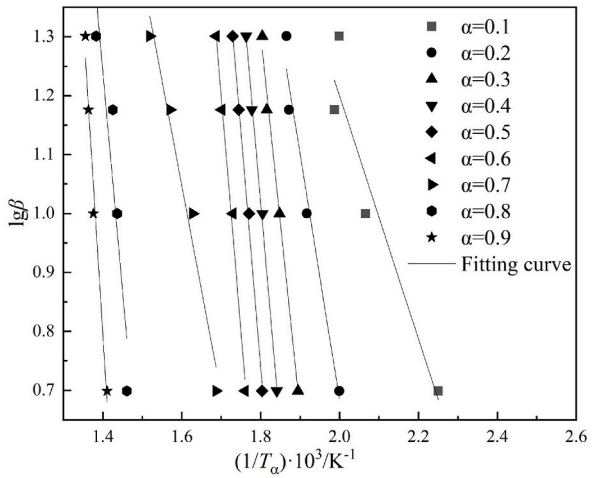

Fig. 8. Fitting curves of lgβ-1/T_α in air atmospheres.

Table 4
Pyrolysis activation energy of ryegrass at different conversion rates.

Atmospheres	α/%	fitted equations	R	E/kJ·mol^{-1}	Average E/kJ·mol^{-1}
N_2	10	Y = −3.76X+10.15	0.7314	68.45	65.39
	20	Y = −3.91X+10.42	0.8372	71.18	
	30	Y = −3.93X+10.41	0.8853	71.54	
	40	Y = −3.84X+10.13	0.9118	69.91	
	50	Y = −3.68X+9.69	0.9058	66.99	
	60	Y = −3.53X+9.27	0.7082	64.26	
	70	Y = −3.38X+8.86	0.9637	61.53	
	80	Y = −3.25X+8.51	0.9986	59.16	
	90	Y = −3.05X+7.96	0.9809	55.52	
Air	10	Y = −2.06X+5.32	0.9178	37.50	116.93
	20	Y = −4.17X+9.02	0.9718	75.91	
	30	Y = −6.41X+12.85	0.9930	116.69	
	40	Y = −7.66X+ 14.81	0.9975	139.45	
	50	Y = −7.98X+ 15.11	0.9958	145.27	
	60	Y = −7.97X+ 14.76	0.9905	145.09	
	70	Y = −3.54X+ 6.71	0.9708	64.44	
	80	Y = −7.44X+ 11.66	0.8592	135.44	
	90	Y = −10.58X+ 15.61	0.9791	192.60	

Table 5
Calculated kinetic equation results by S–S method.

Atmospheres	$G(\alpha)$	Es/kJ·mol^{-1}	lgAs/min^{-1}	R^2	Es/kJ·mol^{-1}	lgAs/min^{-1}	R^2	Es/kJ·mol^{-1}	lgAs/min^{-1}	R^2	Es/kJ·mol^{-1}	lgAs/min^{-1}	R^2
N_2		5 K min $^{-1}$			10K· min $^{-1}$			15K· min $^{-1}$			20K· min $^{-1}$		
	1	28.40	7.49	0.9789	24.39	5.42	0.9617	22.57	5.44	0.9242	20.57	5.37	0.9151
	2	19.30	4.69	0.9715	16.02	4.71	0.9473	14.56	4.78	0.9051	13.11	4.79	0.8963
	3	4.73	3.77	0.9681	4.00	4.04	0.9413	3.64	4.22	0.8976	3.09	4.38	0.8890
	4	6.01	3.79	0.9603	4.73	4.06	0.9286	4.37	4.22	0.8823	3.82	4.34	0.8743
	5	19.66	4.99	0.9902	19.30	5.24	0.9972	19.11	5.38	0.9885	18.02	5.41	0.9852
	6	22.21	5.27	0.9891	22.21	5.54	0.9974	22.03	5.68	0.9905	20.94	5.70	0.9874
	7	6.01	3.79	0.9603	4.73	4.06	0.9286	4.37	4.22	0.8823	3.82	4.34	0.8743
	8	12.20	4.12	0.9297	8.74	4.20	0.8856	4.65	4.32	0.8342	6.55	4.40	0.8289
	9	66.07	8.69	0.9861	53.16	8.26	0.9782	50.24	8.13	0.9513	46.06	7.84	0.9457
	10	47.88	7.67	0.9912	44.78	7.62	0.9918	43.51	7.63	0.9747	40.41	7.47	0.9702
	11	39.50	6.99	0.9916	38.04	7.09	0.9959	37.32	7.17	0.9838	34.95	7.08	0.9801
	12	28.95	6.15	0.9905	28.76	6.40	0.9978	28.58	6.51	0.9909	27.12	6.50	0.9880
	13	82.65	10.54	0.8341	46.97	7.38	0.7564	37.14	6.65	0.6994	28.22	5.99	0.6940
	14	22.94	5.69	0.9893	23.12	5.97	0.9980	22.94	6.12	0.9935	21.85	6.14	0.9912
	15	76.64	10.07	0.9464	67.89	9.50	0.9082	61.15	9.02	0.8588	54.24	8.49	0.8520
	16	81.37	10.44	0.8906	52.98	7.97	0.8268	44.24	7.32	0.7683	35.86	6.68	0.7619
	17	22.03	5.01	0.9896	20.39	5.16	0.9883	19.66	5.25	0.9675	18.02	5.26	0.9620
	18	32.22	6.38	0.9529	36.59	6.99	0.9803	37.87	7.25	0.9940	36.96	7.28	0.9962
	19	36.59	6.63	0.9769	38.59	7.03	0.9940	38.78	7.20	0.9939	37.32	7.17	0.9919
	20	26.03	5.94	0.9213	31.86	6.66	0.9572	33.86	6.98	0.9833	33.31	7.05	0.9902
	21	16.20	4.50	0.9888	14.75	4.68	0.9854	14.20	4.80	0.9625	13.11	4.84	0.9569
	22	12.74	4.24	0.9883	11.65	4.43	0.9837	11.10	4.57	0.9598	10.19	4.64	0.9542
	23	32.40	6.06	0.9891	31.31	6.22	0.9942	30.58	6.31	0.9801	28.95	6.25	0.9752
	24	31.86	5.88	0.9869	28.95	5.88	0.9818	27.67	5.92	0.9555	25.48	5.85	0.9482
	25	25.30	5.67	0.9840	26.21	5.99	0.9964	26.40	6.15	0.9949	25.12	6.18	0.9928
	26	19.18	5.32	0.9806	20.75	5.68	0.9945	21.12	5.86	0.9971	20.21	5.90	0.9962
	27	15.84	5.09	0.9785	17.11	5.45	0.9931	17.29	5.64	0.9976	16.75	5.70	0.9972
	28	116.33	15.27	0.9669	93.21	13.19	0.9465	85.02	12.50	0.9096	75.55	11.69	0.9055
	29	116.33	14.27	0.9669	93.21	12.19	0.9456	85.02	11.50	0.9096	75.55	10.69	0.9055
	30	41.51	7.79	0.9784	32.59	7.20	0.9642	32.40	7.37	0.9318	29.31	7.22	0.9268
Air	1	28.76	5.53	0.9881	26.58	5.61	0.9704	17.84	5.70	0.9545	22.94	5.58	0.9332
	2	19.84	4.73	0.9827	17.66	4.85	0.9610	15.66	4.87	0.9417	14.75	4.91	0.9164
	3	4.92	3.76	0.9799	4.37	4.05	0.9568	3.82	4.23	0.9364	3.46	4.38	0.9097
	4	6.19	3.79	0.9731	5.28	4.07	0.9478	4.73	4.23	0.9251	4.37	4.45	0.8959
	5	19.48	4.98	0.9887	19.66	5.28	0.9913	19.48	5.42	0.9915	19.30	5.53	0.9891
	6	22.03	5.27	0.9865	22.57	5.58	0.9908	22.39	5.73	0.9920	22.39	5.83	0.9905
	7	6.19	3.79	0.9731	5.28	4.07	0.9478	4.73	4.23	0.9252	4.37	4.45	0.8959
	8	12.74	4.16	0.9445	10.38	4.29	0.9146	8.56	4.36	0.8867	7.65	4.44	0.8513
	9	60.80	8.78	0.9927	56.98	8.65	0.9814	52.98	8.40	0.9719	50.97	8.31	0.9578
	10	47.88	7.70	0.9938	46.79	7.83	0.9896	44.97	7.80	0.9855	43.87	7.81	0.9779
	11	39.32	6.99	0.9921	39.14	7.22	0.9915	38.23	7.28	0.9899	37.87	7.35	0.9855
	12	28.76	6.14	0.9885	29.13	6.45	0.9918	28.95	6.59	0.9927	28.95	6.68	0.9911
	13	10.48	11.31	0.8525	61.53	8.79	0.8077	43.87	7.27	0.7638	37.14	6.77	0.7184
	14	22.57	5.68	0.9861	23.30	6.01	0.9913	23.30	6.16	0.9933	23.48	6.28	0.9932
	15	79.74	10.40	0.9604	66.63	9.37	0.9325	56.25	8.53	0.9069	51.52	8.18	0.8743
	16	86.84	11.00	0.9076	65.35	9.16	0.8691	50.43	7.92	0.8313	44.42	7.45	0.7878
	17	22.03	5.03	0.9932	21.30	5.25	0.9871	20.39	5.32	0.9812	19.84	5.39	0.9715
	18	30.95	6.29	0.9346	35.13	6.89	0.9662	37.50	7.23	0.9805	38.59	7.43	0.9894

(*continued on next page*)

Table 5 (*continued*)

Atmospheres	$G(\alpha)$	Es/kJ·mol^{-1}	lgAs/min^{-1}	R^2	Es/kJ·mol^{-1}	lgAs/min^{-1}	R^2	Es/kJ·mol^{-1}	lgAs/min^{-1}	R^2	Es/kJ·mol^{-1}	lgAs/min^{-1}	R^2
	19	35.68	6.58	0.9679	38.23	7.04	0.9834	39.14	7.26	0.9892	39.50	7.39	0.9916
	20	24.76	5.84	0.8949	29.49	6.50	0.9413	32.77	6.92	0.9637	34.59	7.17	0.9781
	21	16.20	4.51	0.9935	15.47	4.76	0.9856	14.75	4.85	0.9785	11.36	5.03	0.9673
	22	12.93	4.24	0.9935	12.38	4.48	0.9847	11.65	4.60	0.9770	11.10	4.70	0.9651
	23	32.22	6.06	0.9889	32.40	6.31	0.9893	31.68	6.40	0.9871	31.13	6.46	0.9816
	24	32.04	5.90	0.9919	30.77	6.06	0.9828	28.95	6.05	0.9738	28.03	6.07	0.9606
	25	24.76	5.65	0.9781	26.03	6.01	0.9879	26.58	6.20	0.9920	26.76	6.31	0.9934
	26	19.11	5.29	0.9726	20.57	5.67	0.9855	21.12	5.87	0.9915	21.48	6.00	0.9949
	27	15.47	5.08	0.9695	16.75	5.44	0.9839	17.29	5.65	0.9907	17.66	5.79	0.9951
	28	119.79	15.66	0.9779	104.31	14.31	0.9591	95.75	13.19	0.9435	91.93	12.71	0.9213
	29	119.79	14.66	0.9779	104.31	13.31	0.9591	95.75	12.19	0.9435	91.93	11.71	0.9213
	30	42.42	7.89	0.9876	38.41	7.77	0.9720	34.77	7.58	0.9593	32.95	7.54	0.9410

Table 6
Selection results for kinetic equations.

Atmospheres	β/K·min^{-1}	$G(\alpha)$	$\lvert(E_S-E_O)/E_O\rvert$	$\lvert(\lg A_S-\lg A_k)/\lg A_k\rvert$
N_2	5	$[-\ln(1-\alpha)]^2$	0.17	0.16
	10		0.04	0.21
	15		0.06	0.25
	20		0.17	0.29
Air	5	$(1-\alpha)^{-1}$	0.02	0.10
	10		0.11	0.18
	15		0.18	0.24
	20		0.21	0.27

degree of ryegrass decreased. In addition, the α_{max} values obtained at different heating rates do not exhibit approaching equality, suggesting that this method is unsuitable for determining the pyrolysis activation energy E of ryegrass.

Refer to Figs. 7 and 8, and Table 4 for the fitting curves and results obtained using the FWO equal conversion method, respectively. Table 4 demonstrates that the straight lines fit more accurately in the air atmosphere compared to the nitrogen atmosphere. When in a nitrogen atmosphere, the pyrolysis activation energy E decreases with the increase of conversion α. However, the fitting results in air atmosphere are completely opposite. The difference between the maximum pyrolysis activation energy and the minimum pyrolysis activation energy in nitrogen atmosphere and air atmosphere is 16.02 kJ/mol and 155.6 kJ/mol, respectively. The activation energy for pyrolysis of ryegrass in the air atmosphere is higher than that in the nitrogen atmosphere. This is due to the exothermic reaction caused by the production of volatiles released during oxidation [36]. The former has a smaller value than the average pyrolysis activation energy (65.39 kJ/mol), whereas the latter has a larger value of (116.39 kJ/mol). The pyrolysis of ryegrass in a nitrogen atmosphere only meets the standard of the International Thermal Analysis Association when the difference between the maximum and minimum activation energy obtained by α is less than the average value [37]. This indicates that this method is not completely appropriate for determining the pyrolysis activation energy of ryegrass.

Table 5 displays the E_S and lg$A$s values calculated using the S–S method. When the reactions take place in either a nitrogen atmosphere or an air atmosphere, the E_S corresponding for all the mechanism functions fall within the range of $0 < E_S < 400$ kJ mol^{-1}. By comparing the screening results of E_O with E_S, lgA_k, and lgA_S (shown in Table 6), it is observed that the mechanism function (15) conforms to both conditions $(E_S-E_O)/E_O \leq 0.22$ and $(\lg A_S-\lg A_k)/\lg A_k \leq 0.30$ in a nitrogen atmosphere. The mechanism function may be expressed as $g(\alpha) = [-\ln(1-\alpha)]^2$. The activation energies E_S at heating rates of 5, 10, 15, and 20 K min^{-1} are 76.64, 67.89, 61.15, and 54.24 kJ mol^{-1}, respectively. The lg(As) is 10.07, 9.50, 9.02, and 8.49min^{-1}, correspondingly. In the air atmosphere, the mechanism function(28) meets the above conditions simultaneously. The function of the mechanism is represented by $g(\alpha)=(1-\alpha)^{-1}$, E_S is 119.79, 104.31, 95.75, and 91.93 kJ mol^{-1}, and lg(As) is 15.66, 14.31, 13.19, and 12.71min^{-1}, respectively.

Through a comparison of the pyrolysis activation energy of ryegrass, calculated by Kissinger method, FWO conversion method, and S–S method under different atmospheres, it has been observed that the pyrolysis activation energy of ryegrass in air atmosphere is higher than that in a nitrogen atmosphere. Additionally, the average weight loss rate is also higher, suggesting that the air atmosphere is more conducive to the pyrolysis of ryegrass.

4. Conclusion

Optimal pyrolysis of ryegrass is achieved with a heating rate of 15 °C/min, while both excessively rapid and slow heating rates are unfavorable. The highest percentage of weight loss rate during pyrolysis occurs at this specific heating rate. In comparison to a nitrogen atmosphere, the percentage of weight loss of ryegrass in air atmosphere is higher and the temperature required for the average percentage of weight loss of complete decomposition is lower. In both atmospheres, the peak height of the DTA curve of ryegrass pyrolysis increased with the increase in heating rate. The FWO equal conversion method is not entirely suitable for determining the activation energy of ryegrass pyrolysis. The mechanisms that are estimated and screened using the S–S method are represented by the functions calculated $g(\alpha) = [-\ln(1-\alpha)]^2$ and $g(\alpha)= (1-\alpha)^{-1}$.

Data availability statement

All data associated with this study is included in the article and/or referenced in the text.

Ethics statement

Ethics committee review and/or approval was not required for this study, as no animal or human-based experiments/case studies were used.

CRediT authorship contribution statement

Yonglin Wu: Writing – original draft, Formal analysis, Data curation, Conceptualization. **Ming Jiang:** Writing – review & editing. **Yichun Liu:** Data curation. **Yishu Deng:** Writing – review & editing, Funding acquisition.

Declaration of competing interest

The authors declare that they have no known competing financial interests or personal relationships that could have appeared to influence the work reported in this paper.

Acknowledgements

The authors gratefully acknowledge the Young Talent Project of Yunnan Revitalization Talent Support Program (No. XDYC-QNRC-2022-0087) and the Major Science and Technology Projects in Yunnan Province (202302AE090012)

References

[1] C. Xu, Q. Wu, Research progress on application of ryegrass and its enlightenment to rocky desertification control, Chin Wild Plant Resour 40 (10) (2021) 66–72.
[2] N. Jiang, S. Yang, J. Yang, Y. Li, Y. Zu, Differences of absorption and accumulation of Cd and as in soil by different cultivars of perennial ryegrass, J Yunnan Agr U 37 (1) (2022) 152–161.
[3] T. Yamada, J.W. Forster, M.W. Humphreys, T. Takamizo, Genetics and molecular breeding in Lolium/Festuca grass species complex, Grassl. Sci. 51 (2005) 89–106.
[4] J. Guo, R. Feng, Y. Ding, R. Wang, Applying carbon dioxide, plant growth-promoting rhizobacterium and EDTA can enhance the phytoremediation efficiency of ryegrass in a soil polluted with zinc, arsenic, cadmium and lead, J Environl Manage 141 (2014) 1–8.
[5] H. Jia, D. Hou, D. O'Connor, S. Pan, J. Zhu, N.S. Bolan, J. Mulder, Exogenous phosphorus treatment facilitates chelation-mediated cadmium detoxification in perennial ryegrass (Lolium perenne L.), J. Hazard Mater. 389 (2020) 121849.
[6] G. Li, F. Chen, S. Jia, Z. Wang, Q. Zuo, H. He, Effect of biochar on Cd and pyrene removal and bacteria communities variations in soils with culturing ryegrass (Lolium perenne L.), Environ Pollut 265 (2020) 114887.
[7] E. Leng, Y. Zhang, Y. Peng, X. Gong, M. Mao, X. Li, Y. Yu, In situ structural changes of crystalline and amorphous cellulose during slow pyrolysis at low temperatures, Fuel 216 (2018) 313–321.
[8] V.C. Venkateswarlu Chintala, Production, upgradation and utilization of solar assisted pyrolysis fuels from biomass-a technical review, Renew Sust Energ Rev 90 (2018) 120–130.
[9] S. Wang, G. Dai, H. Yang, Z. Luo, Lignocellulosic biomass pyrolysis mechanism: a state-of-the-art review, Prog Energy Combust 62 (2017) 33–86.
[10] Đ. Katnić, M. Marinović-Cincović, S.J. Porobić, I. Vujčić, A. Šaponjić, B. Sikirić, D. Živojinović, Characterization and kinetics of thermal decomposition behavior of plum and fig pomace biomass, J. Clean. Prod. 352 (2022) 131637.
[11] A. Khan, S.Y. Alghamdi, A.S. Almuflih, A. Abdulrahman, K.M. Qureshi, N. Almakayeel, M.R.N. Qureshi, Analysis of thermal decomposition kinetics of chicken feather fiber reinforced Poly-lactic acid composites filament, Heliyon 10 (2024) e24245.
[12] H.K. Balsora, S. Kartik, T.J. Rainey, A. Abbas, J.B. Joshi, A. Sharma, A.G. Chakinala, Kinetic modelling for thermal decomposition of agricultural residues at different heating rates, Biomass Conversn Bior (2023) 1–15.
[13] R. Huang, Z. Teng, S. Li, Gaussian model analysis and thermal decomposition kinetics of nature fibers, J. Clean. Prod. 357 (2022) 131784.
[14] Y.-C. Chien, T.-C. Yang, K.-C. Hung, C.-C. Li, J.-W. Xu, J.-H. Wu, Effects of heat treatment on the chemical compositions and thermal decomposition kinetics of Japanese cedar and beech wood, Polym. Degrad. Stabil. 158 (2018) 220–227.
[15] M.M. Alashmawy, H.S. Hassan, S.A. Ookawara, A.E. Elwardany, Thermal decomposition characteristics and study of the reaction kinetics of tea-waste, Biomass Conversn Bior 13 (2023) 9487–9505.
[16] S. Gupta, G.K. Gupta, M.K. Mondal, Thermal degradation characteristics, kinetics, thermodynamic, and reaction mechanism analysis of pistachio shell pyrolysis for its bioenergy potential, Biomass Convers Bior 12 (2022) 4847–4861.
[17] J. Robinson, E. Binner, D.B. Vallejo, N.D. Perez, K. Al Mughairi, J. Ryan, B. Shepherd, M. Adam, V. Budarin, J. Fan, Unravelling the mechanisms of microwave pyrolysis of biomass, Chem Eng J 430 (2022) 132975.
[18] S. Sobek, S. Werle, Kinetic modelling of waste wood devolatilization during pyrolysis based on thermogravimetric data and solar pyrolysis reactor performance, Fuel 261 (2020) 116459.
[19] T.A. Vo, Q.K. Tran, H.V. Ly, B. Kwon, H.T. Hwang, J. Kim, S.-S. Kim, Co-pyrolysis of lignocellulosic biomass and plastics: a comprehensive study on pyrolysis kinetics and characteristics, J. Anal. Appl. Pyrol. 163 (2022) 105464.
[20] C.J. Wrasman, A.N. Wilson, O.D. Mante, K. Iisa, A. Dutta, M.S. Talmadge, D.C. Dayton, S. Uppili, M.J. Watson, X. Xu, Catalytic pyrolysis as a platform technology for supporting the circular carbon economy, Nat. Catal. 6 (2023) 563–573.
[21] H. Wang, Evaluation of nutritional value of different types of ryegrass, Chin Feed (08) (2021) 13–16.
[22] X. Guo, J. Zhang, F. Zhan, Y. He, B. Li, M. Jiang, Thermal decomposition characteristics and kinetics of tea stalk, Chem. Ind. For. Prod. 38 (2) (2018) 119–125.
[23] H. Xie, X. Ning, G. Qiu, J. Deng, Mechanism of pyrolysis of sawdust biomass to produce highly reducing gas, Chinese Journal of Environmental Engineering 16 (5) (2022) 1639–1648.
[24] P. Lang, P. Liu, Y. Li, Y. Li, T. Lie, Study on kinetics and thermodynamic parameters for pyrolysis of different sawdust biomass, Chin Forest Prod Ind 59 (7) (2022) 30–37+52.
[25] Y. Xiaodan, M. Liping, Z. Bin, Z. Dalong, L. Yan, Reaction mechanism process analysis with phosphogypsum decomposition in multiatmosphere control, Ind. Eng. Chem. Res. 53 (50) (2014) 19453–19459.
[26] S. Yuan, J. Yang, G. Zhou, F. Xie, B. Tian, D. Wu, X. Hou, X. Huang, H. He, Thermal decomposition process and kinetics of cerium oxalate decahydrate, Chem. Ind. Eng. 38 (4) (2021) 1–12.
[27] M. Huang, S. Lv, C. Zhou, Thermal decomposition kinetics of glycine in nitrogen atmosphere, Thermochim. Acta 552 (2013) 60–64.
[28] Y. Wu, J. Chen, W. Zhang, Q. Jiang, M. Jiang, Comparison of thermal dehydration characteristics and kinetic analysis of phosphogypsum under different atmospheres, Chem. Eng. 36 (2022) 16–20.
[29] M.A. Henrique, W.P.F. Neto, H.A. Silvério, D.F. Martins, L.V.A. Gurgel, H. da Silva Barud, L.C. de Morais, D. Pasquini, Kinetic study of the thermal decomposition of cellulose nanocrystals with different polymorphs, cellulose I and II, extracted from different sources and using different types of acids, Ind. Crop. Prod. 76 (2015) 128–140.
[30] R. Gao, L. Zhan, J. Guo, Z. Xu, Research of the thermal decomposition mechanism and pyrolysis pathways from macromonomer to small molecule of waste printed circuit board, J. Hazard Mater. 383 (2020) 121234.
[31] J. Qie, W. Li, C. Zhou, Research on thermal decomposition kinetics of N,N'-Ethylenebis (stearamide), J Chem Eng Chin Uni 30 (5) (2016) 1112–1118.
[32] L. Zhang, Thermal stability and decomposition kinetics of polysuccinimide, Am J Analyt Chem 4 (2013) 749.
[33] B. Li, E. Jiang, M. Wang, Q. Zhang, Pyrolysis characteristics and kinetic analysis of elephantgrass, Acta Energiae Sol Sinica 32 (12) (2011) 1725–1729.
[34] R.K. Singh, T. Patil, A.N. Sawarkar, Pyrolysis of garlic husk biomass: physico-chemical characterization, thermodynamic and kinetic analyses, Bioresource Technol Rep 12 (2020) 100558.

[35] R. Xiao, W. Yang, X. Cong, K. Dong, J. Xu, D. Wang, X. Yang, Thermogravimetric analysis and reaction kinetics of lignocellulosic biomass pyrolysis, Energy 201 (2020) 117537.
[36] Y.J. Rueda-Ordóñez, K. Tannous, Drying and thermal decomposition kinetics of sugarcane straw by nonisothermal thermogravimetric analysis, Bioresource Technol 264 (2018) 131–139.
[37] S. Vyazovkin, A.K. Burnham, J.M. Criado, L.A. Pérez-Maqueda, C. Popescu, N. Sbirrazzuoli, ICTAC Kinetics Committee recommendations for performing kinetic computations on thermal analysis data, Thermochim. Acta 520 (2011) 1–19.